Dynamics of supercooled water in configuration space

E. La Nave,[1] A. Scala,[1,2] F. W. Starr,[1] H. E. Stanley,[1] and F. Sciortino[2]
[1]*Center for Polymer Studies and Department of Physics, Boston University, Boston, Massachusetts 02215*
[2]*Dipartmento di Fisica e INFM, Universitá di Roma "La Sapienza" Piazzale Aldo Moro 2, I-00185, Roma, Italy*
(Received 1 February 2001; published 8 August 2001)

We study the potential energy surface (PES) sampled by a liquid modeled via the widely studied extended simple point charge (SPC/E) model for water. We characterize the curvature of the PES by calculating the instantaneous normal mode (INM) spectrum for a wide range of densities and temperatures. We discuss the information contained in the INM density of states, which requires additional processing to be unambiguously associated with the long-time dynamics. For the SPC/E model, we find that the slowing down of the dynamics in the supercooled region—where the ideal mode coupling theory has been used to describe the dynamics—is controlled by the reduction in the number of directions in configuration space that allow a structural change. We find that the fraction $f_{\rm dw}$ of the double-well directions in configuration space determines the value of the diffusion constant *D*, thereby relating a property of the PES to a macroscopic dynamic quantity; specifically, it appears that $\sqrt{D}$ is approximately linear in $f_{\rm dw}$. Our findings are consistent with the hypothesis that, at the mode coupling crossover temperature, dynamical processes based on the free exploration of configuration space vanish, and processes requiring activation dominate. Hence, the reduction of the number of directions allowing free exploration of configuration space is the mechanism of diffusion implicitly implemented in the ideal mode coupling theory. Additionally, we find a direct relationship between the number of basins sampled by the system and the number of free directions. In this picture, diffusion appears to be related to geometrical properties of the PES, and to be entropic in origin.

DOI: 10.1103/PhysRevE.64.036102 PACS number(s): 66.10.Cb, 61.43.Fs, 64.70.Pf

I. INTRODUCTION

Computer studies of models of liquids have focused on the slowing down of dynamics approaching the glass transition [1], and on the role of the structure of the configurational space in the supercooled states [2–7]. Weakly supercooled states, in which the dynamics are four or five orders of magnitude slower than in normal liquid, have been thoroughly investigated via computer simulations [8–12]. The time dependence of several correlation functions has been evaluated over time intervals spanning more than five orders of magnitude. These correlation functions have been compared [13,14], without fitting parameters, with theoretical predictions based on the ideal mode coupling theory [15] for supercooled liquids. The outcome of these studies suggests that the ideal mode coupling theory adequately describes the long-time dynamics of weakly supercooled states, even in network-forming liquids [10,12,16–18].

Parallel studies on the potential energy surface (PES) probed by the liquid are also contributing to the understanding of the origin of the slowing down of the dynamics. These approaches have called attention to various aspects of the PES, including the progressive deepening [3,19] of the potential energy of the local minima [20] visited by the liquid on cooling and the progressive reduction of the number of local minima and their connectivity [21,22].

One approach to understanding the role of the PES is to study the connectivity between different local configurations using the instantaneous normal mode (INM) formalism [23]. Analogous to the standard normal mode theory for solids, an instantaneous normal mode is the eigenfunction of the Hessian, the matrix of the second derivative of the potential energy, with respect to the molecular coordinates. In a liquid state, the eigenvalues of the Hessian matrix are generally not all positive; the negative eigenvalues indicate a downward curvature of the PES, i.e., indicate unstable directions for the system. Previous studies using the INM formalism indicate that the number of directions with negative curvature is reduced on cooling, and this has motivated theories that relate diffusion in liquids to the INM density of states [24,25]. Low temperature liquid dynamics involve the superposition of fast oscillations around quasiequilibrium positions (intrabasin motion) and the rearrangement of the system between these positions (interbasin motion) [26]. The typical oscillation period is much shorter than the typical time needed by the system to rearrange itself, i.e., the structural relaxation time. INM theories for diffusion relate the diffusion of the system to activated processes of interbasin motion in configuration space. In this respect, the imaginary modes are considered representative of the barriers crossed when the system changes basins.

More recently, it has become clear that the information contained in the INM density of states requires further processing before being unambiguously associated with the long-time dynamics [27–30]. More specifically, one must select the imaginary modes that are actually related to diffusion in configuration space. This detailed analysis has recently been carried out in a few systems [27]. At the same time, it has been found that, in the appropriate temperature range, activated processes are not required for structural rearrangement, and diffusion can occur via exploration of low potential energy pathways [5,22,29]. This mechanism—which

we refer to as ''free exploration in configuration space''—appears to be the dominant mechanism for diffusion in weakly supercooled states. It has been hypothesized [29] that the reduction in the number of directions allowing free exploration of configuration space is the mechanism of diffusion implicitly implemented in the ideal mode-coupling theory (MCT) [15]. The crossover between MCT dynamics and activated dynamics as T is decreased toward the MCT critical temperature would be related to the vanishing number of directions of free exploration on cooling. Indeed, a recent calculation of the location on the PES of the *closest* saddle [21,31] suggests that, in the weakly supercooled states, the order [32] of the closest saddle decreases and approaches zero at the MCT critical temperature. In this picture, diffusion appears to be related to geometrical properties of the PES and hence, to be entropic in origin.

In this paper, we report an extensive INM study of a rigid model for water, the SPC/E [33,34]. We study in detail the supercooled region of this potential for 30 state points (6 different densities and 5 temperatures). A preliminary account of some of the present results has been published in Ref. [22].

The reasons for selecting the SPC/E potential are twofold.

(i) The structural, dynamic, and thermodynamic properties of the SPC/E model have been studied in detail, and it has been found that the model reproduces the anomalous pressure and temperature dependence of several quantities. In the region studied, the SPC/E dynamics follows closely the predictions of MCT [12,16]. Several properties of the PES have been calculated, and recently the $(\rho,\ T)$ dependence of the configurational entropy has been calculated, and shown to correlate with the dynamic behavior [6].

(ii) As observed experimentally, the SPC/E model has a maximum of the diffusion constant D upon compressing at constant temperature [35]. The maxima in the diffusion constant D can be exploited as a sensitive probe for testing proposed relations between the change in topology of configuration space and the change in D, allowing identification of a precise correspondence between diffusion and PES properties.

The paper is organized as follows. In Sec. II, we review the INM formalism that we employ. In Sec. III we give the computational details. We present the results in Sec. IV, which is divided into subsections detailing the INM density of states and the relationship to dynamic properties. In Sec. V we present the conclusions.

II. INSTANTANEOUS NORMAL MODES

A. Definition of instantaneous normal modes

Instantaneous normal modes are defined in analogy with the standard normal mode analysis for a solid. We consider a system consisting of N rigid molecules at a given temperature T and volume V. As coordinates for all N molecules in the $6N$-dimensional configurational space we choose the center of mass position and the angles connected to rotations around the three principal axes (see Ref. [36] for a discussion on the effects of different coordinate choices). The instantaneous normal modes are the eigenvectors obtained by the diagonalization of the Hessian matrix $\mathbf{H}$ (the $6N\times 6N$ matrix of second derivatives of the potential energy), and the eigenvalues of the Hessian are the squares of the corresponding frequencies ω associated with each mode. Typical liquid configurations are not local minima of the potential energy. Therefore not all the eigenvalues of the matrix $\mathbf{H}$ will be positive.

One can interpret a negative eigenvalue as the square of an imaginary frequency, and carry on the analysis in analogy with what is done for solids. The INM can be classified as stable (the modes corresponding to a real frequency) and unstable (the modes corresponding to an imaginary frequency). If the eigenmodes of the system do not decorrelate with time, then modes with real frequency would correspond to a stable oscillator $\cos(\omega t)$ while modes with imaginary frequency would exhibit unstable growth $\cosh(\omega t)$.

The short time dynamics can be rebuilt from the knowledge of the INM's [37]. The average density of states $\langle \pi(\omega)\rangle$ can be decomposed as the sum of the density of states $\langle \pi_s\rangle$ for stable modes and the density of states $\langle \pi_u\rangle$ for unstable modes,

$$\langle \pi(\omega)\rangle = \left\langle \sum_{i=1}^{N}\sum_{\alpha=1}^{6} \delta(\omega-\omega_{i\alpha}) \right\rangle = \langle \pi_s\rangle + \langle \pi_u\rangle. \quad (1)$$

By convention, the *imaginary* frequency modes are represented as *negative* frequencies, so $-\omega$ represents an imaginary frequency mode $i\omega$.

B. Instantaneous normal modes and topology of the PES

In the very early INM studies [25], directions in configurational space with negative curvature were associated with diffusive directions, i.e., with directions along which the motion of the system produces a structural change in real space; in configuration space, a structural change corresponds to a change of basin of the PES. The total fraction f_u of unstable directions (were the subscript u stands for unstable) has been related to D [23]. It was realized that even for configurations with virtually no diffusion, e.g., deeply quenched glassy configurations or even crystalline states [28,30,38], a nonnegligible number of imaginary modes is still present, demonstrating that anharmonicities in the potential energy contribute to the fraction of unstable modes. Thus the information contained in the INM density of states requires further processing before being unambiguously associated with the process of diffusion.

Many methods have been proposed for separating the diffusive modes (basin changes in configuration space) from the nondiffusive modes (no basin changes) [27,28,38]. One approach is to classify the modes according to their potential energy profile (Fig. 1), and partition those unstable modes into two groups: (i) imaginary normal modes due to the anharmonicities (shoulder modes, with fraction f_{sh}) and (ii) modes along which the system is crossing a saddle (double-well modes, with fraction f_{dw}) [28]. In order to distinguish between shoulder and double-well modes, the potential energy profile is calculated along straight paths, which follow the direction of the eigenvector. By calculating the energy

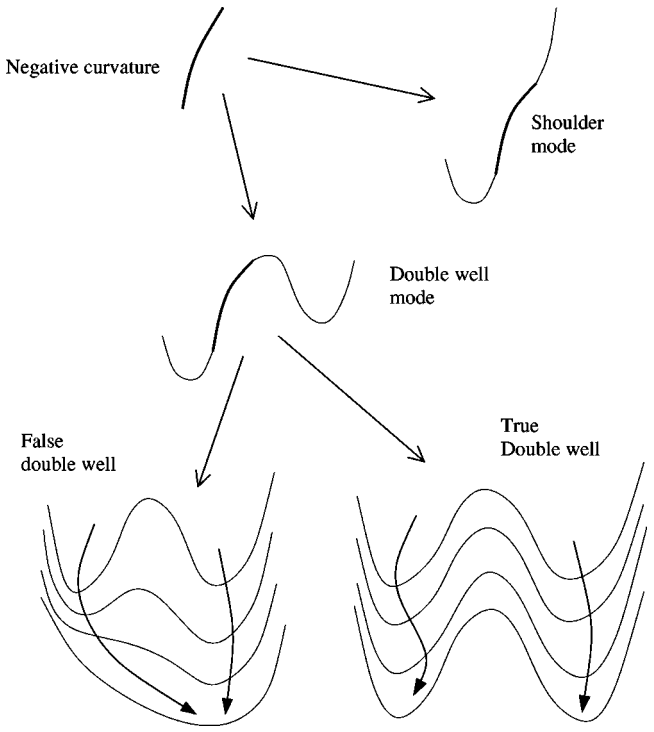

FIG. 1. Schematic sketch of the possible shapes of the PES associated with imaginary eigenvalues. Unstable modes are first separated into shoulder and double-well modes. Furthermore, double-well modes are split into diffusive (true double well) and nondiffusive ones (false double well).

along this path, one can distinguish double-well modes from shoulder modes. Although the INM eigenfunctions change substantially in the process of calculating the energy profile [39], the eigenfunctions used to obtain the profile are not recalculated along the path.

In a dense liquid, any straight direction in configuration space will ultimately bring together an arbitrary pair of neighboring atoms, and the repulsive force between them will cause the energy profile to rise sharply with positive curvature. This rise of the potential energy (due to the straight path approximation) has two major consequences: (i) some modes whose true energy profile (evaluated along a curvilinear path, not a straight line) would suggest classification as a double-well mode will appear as a shoulder mode [Fig. 2(a)], (ii) the energy profile of double-well modes is strongly affected by the straight path approximation [Fig. 2(b)]. Indeed, both the estimation of the location of the minima and of the saddle barrier heights are underestimated by the straight path approximation [24].

These features—which apparently weaken the INM approach and seem to question whether the INM analysis can predict characteristic structural times in the system—are actually quite useful. In fact, they select the directions along which the system is very near to a saddle and hence the directions along which a basin change is happening. Therefore, despite the error inherent in the straight path approximation, f_{dw} is a meaningful quantity that correlates well with D.

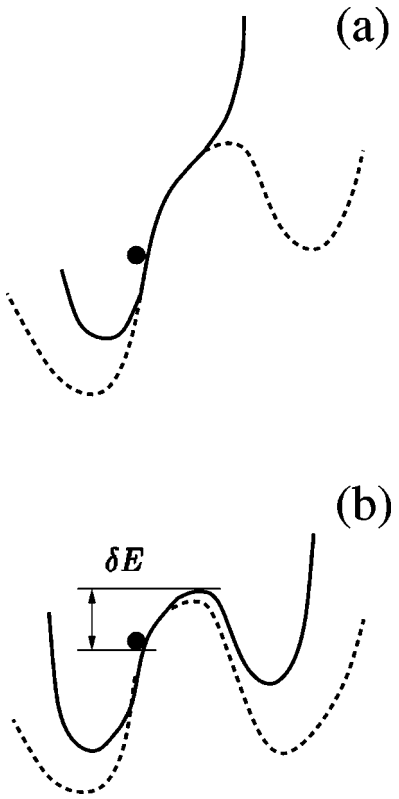

FIG. 2. Schematic sketch of the pitfalls associated with the straight path approximation, on calculating the energy profile. Lower (upper) sketch shows the case when the location of the instantaneous configuration is close to (far from) a saddle point. The net effect of the straight path approximation is an artificial rise of the potential energy profile with negative curvature.

Consistent with this picture is the fact that the calculated difference δE [see Fig. 2(b)] in the energy between the location of the point and the ridge is found to be much smaller than $k_B T$ (where k_B is the Boltzmann constant). Thus the double-well classification is able to sort out the diffusive modes even if no physical meaning can be attributed to the calculated straight-path approximation energy profile.

Some researchers [30,40] have pointed out that even modes classified as double-well can involve intrabasin motions—which, if true, renders the classification based on the straight-path energy profile problematic. As shown in Fig. 1, the steepest descent paths (starting from the two distinct one-dimensional minima detected) may indeed lead to the same local minima. To remove such spurious nondiffusive contributions to f_{dw}, Gezelter *et al.* [30] suggested that a minimization starting from the two apparent minima must be performed for each double-well mode. According to this method, the double-well mode under study is considered diffusive only if the procedure leads to two different minima.

An alternative way of distinguishing diffusive double-well modes from nondiffusive modes is based on the localization properties of the eigenvectors. Bembenek and Laird [28] have suggested that modes that are nonlocalized are diffusive. To support their hypothesis, Bembenek and Laird have studied the participation ratio p_α of each mode α [41].

In studying the size dependence of p_α in a soft-sphere system, they have been able to distinguish diffusive nonlocalized modes from nondiffusive ones. In their model they indicate that the estimated liquid-glass transition is associated with the temperature below which all the unstable modes become localized, and that the crossover between stable and unstable modes occurs at a nonzero imaginary frequency. Unfortunately, due to a limitation in computational resources, they associated this localization transition with falling out of equilibrium, rather than with a crossover in the dynamics at the mode coupling temperature [28]. This type of analysis is very time consuming, since it requires finite-size studies that are not feasible for the complicated potential and the long trajectories that we study here. For this reason we have not applied the approach proposed in Ref. [28].

III. COMPUTATIONAL DETAILS

We study a system composed of 216 water molecules interacting via the SPC/E potential [33]. We analyze recent simulations for six densities between 0.95 and 1.3 g/cm^3 and for each density five temperatures [12]. To achieve equilibration at the lowest temperatures and to generate independent configurations, we extended the molecular dynamics runs up to 200 ns, corresponding to 200 million integration time steps. Simulation details are found in Ref. [12].

For each state point, we extract 100 equally spaced configurations from which we calculate and diagonalize the Hessian, using the center of mass and the three principal inertia momenta vectors as molecular coordinates [42]. We also compare the INM properties of the liquid with those of the crystalline state (ice I_h) at several densities. Details of the ice simulations are given in Ref. [43].

We diagonalize the Hessian matrix using standard LAPAK routines [44]. For each unstable-mode eigenvector, we calculate the potential energy profile along the straight eigenvector path and classify the imaginary modes into two categories, shoulder modes, and double-well modes [28]. The modes are classified as shoulder modes when no second minimum is found within an energy range of 10 kJ/mol.

IV. RESULTS

A. Instantaneous normal mode DOS

Water is one of the first liquids whose INM density of states (DOS) has been calculated and for which the T dependence of f_u has been estimated [22,29,45]. We show the INM DOS for the SPC/E water in Fig. 3. The stable modes of the INM DOS can be partitioned rather clearly into hindered translations (below 400 cm^{-1}) and hindered rotations (above 400 cm^{-1}). The unstable modes are distributed around a single peak at ≈ -60 cm^{-1}. Figure 3(c) shows also the DOS of the SPC/E ice I_h where the translational and rotational bands are better resolved. We note that, even in the crystalline states, the number of unstable modes (i.e., the area under the negative frequencies peak) is close to the number of negative modes in supercooled liquid states, a clear indication that there are many negative modes that are not related to the system diffusion. Partitioning the DOS into the contributions of the shoulder modes and of the double-well modes [shown in Fig. 3(d) for one selected state point], we can identify a lower frequency cutoff $|\omega_c| \approx 30$ cm^{-1} below which the density of states of the double-well modes vanishes. This finding is consistent with previous observations [25,38] that modes with $|\omega| \leqslant |\omega_c|$ do not contribute to diffusive processes since they are mainly due to anharmonicities of the PES.

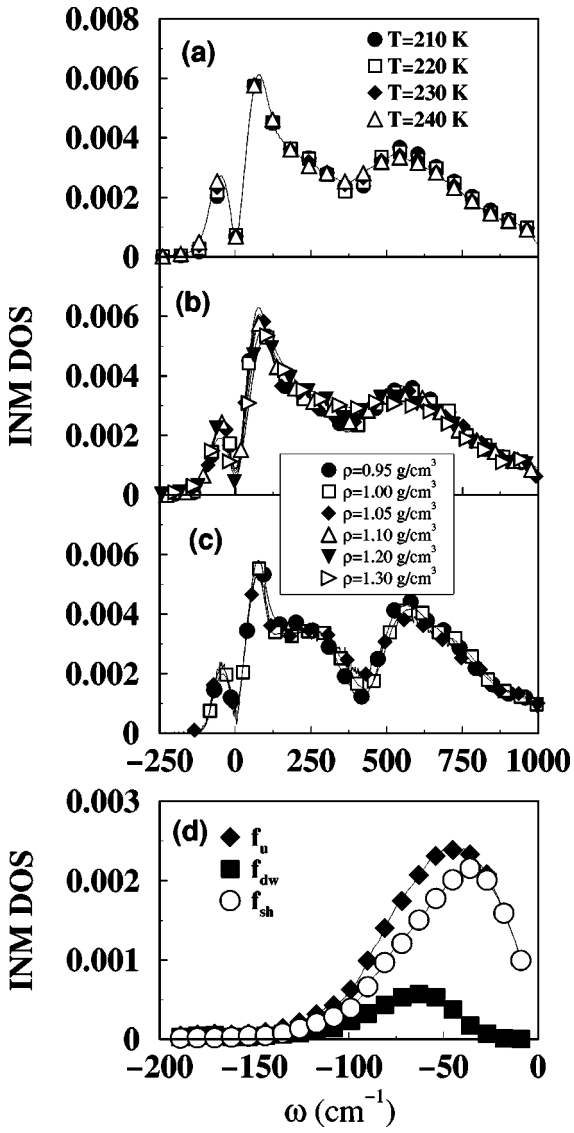

FIG. 3. Instantaneous normal modes density of states for SPC/E water. (a) T dependence at $\rho = 1.0$ g/cm^3, (b) ρ dependence at $T = 210$ K, (c) ρ dependence for SPC/E ice I_h, and (d) density of states of the unstable modes partitioned into shoulder and double-well modes at $T = 210$ K and $\rho = 1.0$ g/cm^3.

Figures 4(a) and 4(b) show the T dependence of the average frequencies of the unstable modes $\langle \omega_u \rangle$ and of the double-well modes $\langle \omega_{\mathrm{dw}} \rangle$. In the studied range of the phase diagram, both average frequencies increase monotonically with T and with ρ. Hence, the anomalous density dependence of D (i.e., the fact that D shows a maximum in ρ) cannot

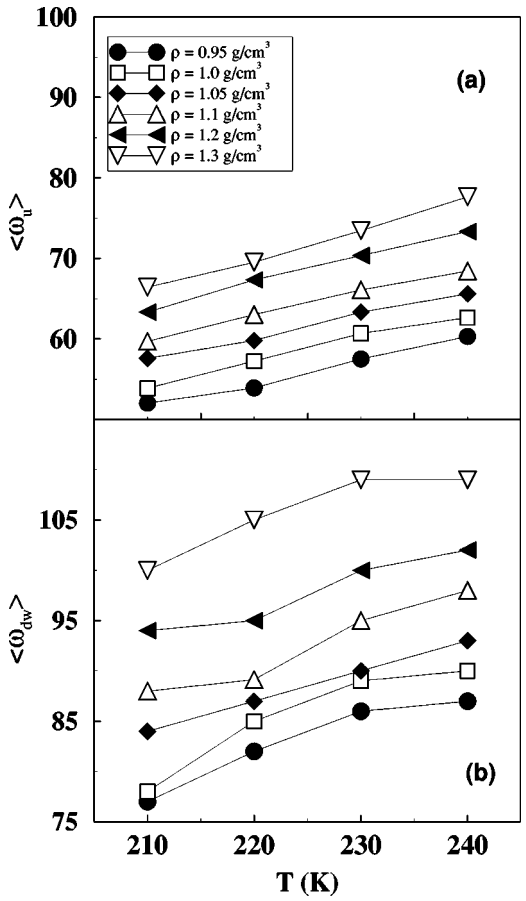

FIG. 4. T dependence of the average frequency (a) of the unstable modes $\langle \omega_u \rangle$ and (b) of the double-well modes $\langle \omega_{\mathrm{dw}} \rangle$.

arise from the ρ dependence of $\langle \omega_u \rangle$ and $\langle \omega_{\mathrm{dw}} \rangle$.

As discussed in Sec. II B, the energy profile reconstructed along a straight path is very different from the curvilinear energy profile. Moreover the potential energy difference δE between the energy of the instantaneous configuration and the energy of the maximum represents an upper limit estimate of the energy required to change basins along a double-well direction. Figure 5 shows the distribution $P(\delta E)$, which follows an approximately exponential law. Figure 5 supports the fact that the system is always located very close to the ridge separating different basins. The average δE is ≈ 1000 times smaller than the value of the thermal fluctuations ($3k_BT \approx 5$ kJ/mol). Hence, energy barriers do not hinder the motion between different basins; the system does not require rare energy fluctuations to change basins, and basin crossing is limited only by the number of possible escape directions to another basin.

Motivated by this, we consider the behavior of the f_{dw}, as well as f_u and f_{sh}. The T and ρ dependence of the fractions of imaginary (unstable) modes f_u, double-well modes f_{dw}, and shoulder modes f_{sh} (where $f_u = f_{\mathrm{dw}} + f_{\mathrm{sh}}$) is shown in Fig. 6. As already noted in Refs. [29,38], $f_{\mathrm{dw}} < f_{\mathrm{sh}}$ for water, while $f_{\mathrm{dw}} \approx f_{\mathrm{sh}}$ for a Lennard-Jones liquid. A possible explanation could be related to the presence of hydrogen bonds in water, which are highly directional interactions. Hence, even a small rotation of one water molecule results in displacement of the proton out from the oxygen-oxygen line, producing a breaking of the bond with an associated energy loss of several kJ/mol and resulting in a dramatic increase of the potential energy along the eigendirection followed. This increase in potential will result in a shoulder mode, as schematically explained in Sec. II B. Such a mechanism does not exist in Lennard-Jones liquids, and so fewer shoulder modes are expected. Hence it is possible that the distortion of the hydrogen bond during the evaluation of the one-dimensional

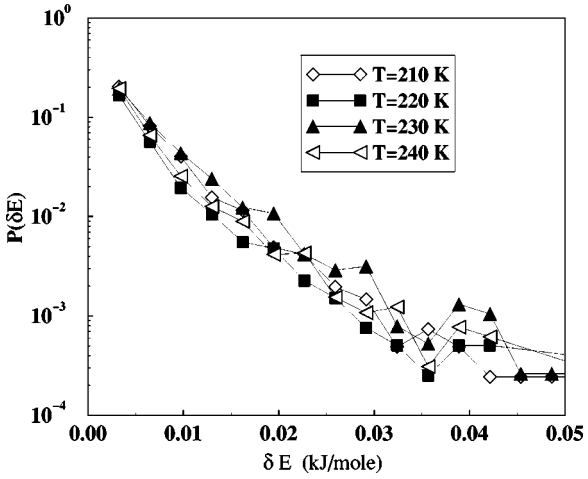

FIG. 5. Distribution of the potential energy difference δE [see Fig. 2(b)] between the energy of the starting configuration and the energy of the one-dimensional saddle.

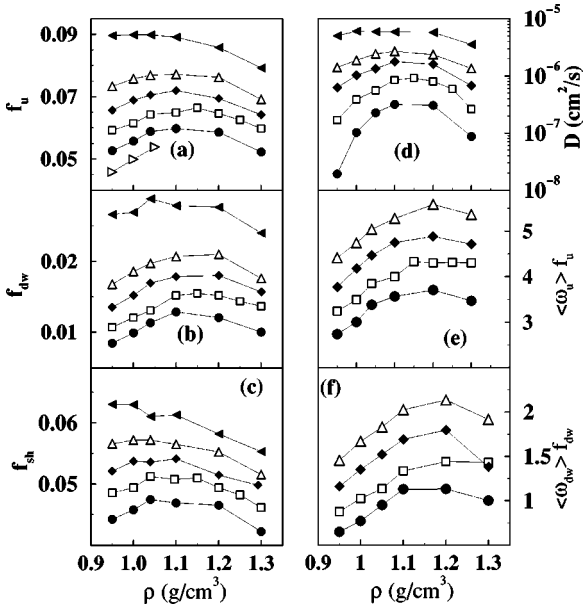

FIG. 6. Density dependence at temperatures of $T = 210$ K (filled ○), $T = 220$ K (□), $T = 230$ K (filled ◇), $T = 240$ K (△), and $T = 260$ K (filled △) of several INM properties: (a) the fraction of imaginary (unstable) modes f_u (also shown by the symbol ◁ is f_u for ice I_h at $T = 210$ K), (b) fraction of double-well modes f_{dw}, (c) fraction of shoulder modes f_{sh}, (d) the diffusion coefficient D [12], (e) product $f_u \langle \omega_u \rangle$, and (f) product $f_{\mathrm{dw}} \langle \omega_{\mathrm{dw}} \rangle$.

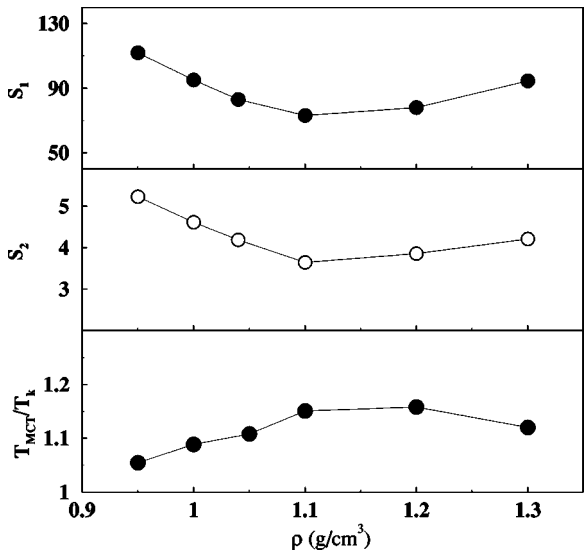

FIG. 7. Density dependence of the quantities $S_1 \equiv (1-f_u) f_{\mathrm{dw}}$ and $S_2 \equiv f_{\mathrm{sh}}/f_{\mathrm{dw}}$ evaluated at $T=210$ K. Also shown is the ratio between the MCT critical temperature T_{MCT} and the Kauzmann temperature T_K at which the extrapolated configurational entropy appears to vanish [47].

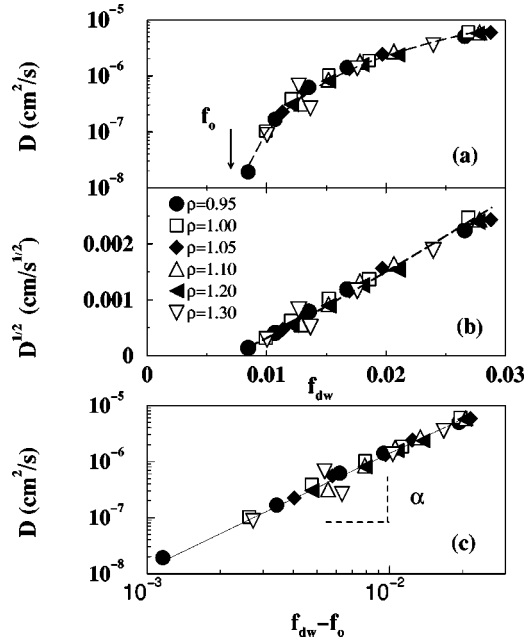

FIG. 8. Plots (a) of $\log D$ versus f_{dw} and (b) of $D^{1/2}$ versus f_{dw}. The dashed line represents a fit using Eq. (5). The arrow indicates the parameter f_0. A log-log plot of D versus f_{dw} is also shown (c).

energy profile may contribute to the abundance of shoulder modes ($f_{\mathrm{sh}} > f_{\mathrm{dw}}$) in water.

On the basis of a comparison between the INM's of water and the ones of a Lennard-Jones liquid CS_2 it has been suggested that the ratio $S_1 \equiv (1-f_u)/f_{\mathrm{dw}}$ and the ratio $S_2 \equiv f_{\mathrm{sh}}/f_{\mathrm{dw}}$ are related to the kinetic behavior of the model itself [38]. It has been speculated that the values of S_1 and S_2 correlate with the degree of ''strength'' (in the strong-fragile Angell nomenclature [46]). The strength of a liquid can been estimated by the ratio between the MCT critical temperature T_{MCT} and the temperature T_K [47] at which the extrapolated configurational entropy appears to vanish. Figure 7 shows S_1, S_2, and T_{MCT}/T_K. We observe a clear anticorrelation between S_1 or S_2 and T_{MCT}/T_K, questioning the previous interpretation of S_1 and S_2 as possible indicators of strength [38].

B. Relationship to diffusion constant

We next discuss the relation between the diffusion constant D and the fraction of imaginary modes. The T and ρ dependence of D is shown in Fig. 6(d). The close correlation of the ρ dependence of f_{dw} and D is striking. At $\rho \approx 1.15$ g/cm^3, f_u and f_{dw} show maxima, supporting the view that f_u and f_{dw} are good indicators of molecular mobility. There is only a weak maximum in f_{sh}, at a slightly lower density $\rho \approx 1.05$ g/cm^3. Therefore we conclude that the presence of the maximum in f_u is mainly due to the contribution of the double-well modes. We attribute the weak maximum in f_{sh} to the occasional erroneous identification of double-well modes as shoulder modes. The presence of maxima in both D and f_{dw} at the same density is a strong indication that f_{dw} is directly related to D, at least for the SPC/E potential.

In the early INM studies [48,49], D was related to the product $f_u \langle \omega_u \rangle$ (or to $f_{\mathrm{dw}} \langle \omega_{\mathrm{dw}} \rangle$). The ρ and T dependence of these two products are shown in Figs. 6(e) and 6(f). We observe that both products have maxima, but for a density that is shifted compared to the D maximum. Hence the data very clearly suggest that f_{dw} (as opposed to $f_{\mathrm{dw}} \cdot \langle \omega_{\mathrm{dw}} \rangle$ or $f_u \cdot \langle \omega_u \rangle$) correlates best with the D data.

To support the hypothesis that f_{dw} is the relevant quantity controlling the dynamics in the range of T and ρ studied, we show D versus f_{dw} for all six isochores studied (Fig. 8). We note that D is a monotonic function of f_{dw}, and that all points fall on the same master curve, covering several orders of magnitude in D. For $D \gtrsim 0.3 \times 10^{-6}$ cm^2/s, the relation between D and f_{dw} is approximately linear, in agreement with the finding of Keyes and co-workers for different liquids [23,24]. The data in Fig. 8 show that, surprisingly, the knowledge of the fraction of double-well directions f_{dw}, is sufficient to determine the value of D, thereby relating a property of the PES to a macroscopic dynamic quantity.

Reference [12] showed for SPC/E that the T dependence of D is well represented by the MCT prediction

$$D \sim (T - T_{\mathrm{MCT}})^{\gamma}, \tag{2}$$

where the diffusivity exponent γ changes between roughly 2.24 and 2.84 with density.

We conjecture that

$$D \sim (f_{\mathrm{dw}} - f_0)^{\alpha}. \tag{3}$$

Figure 8 shows that this conjecture is consistent with our calculations of f_{dw} and D. The best-fit values of the fitting parameters are $f_0 = 0.007 \pm 0.001$ and $\alpha = 2.0 \pm 0.2$. Within the numerical error, D depends on ρ only via the ρ depen-

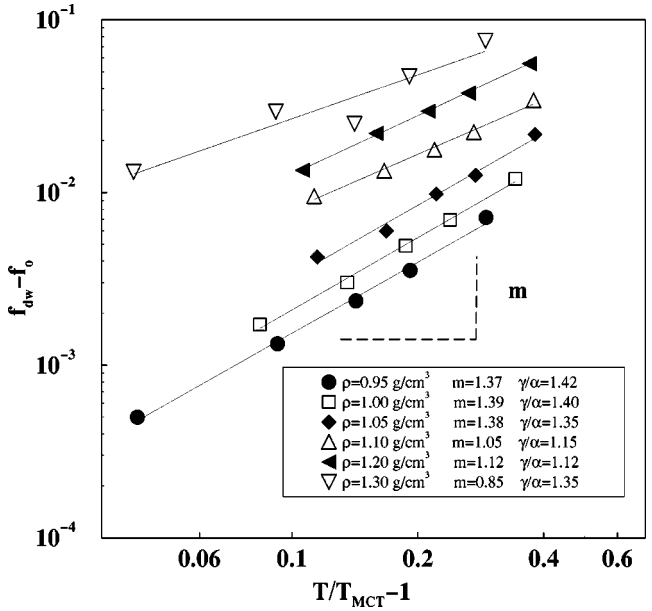

FIG. 9. Log-log plot of $f_{\rm dw}-f_0$ vs $T/T_{\rm MCT}-1$. The lines have been shifted for clarity. Consistency between the power law fit $D\sim(T-T_{\rm MCT})^{\gamma}$ and $D=D_o(f_{\rm dw}-f_0)^{\alpha}$ requires the exponent m in the figure to be equal to γ/α.

dence of $f_{\rm dw}$. Thus the functional form of Eq. (3) supports an apparent universal relation connecting dynamics in real space to a property of the PES.

Equations (2) and (3) imply that exists a nonuniversal, density-dependent power-law relation between $f_{\rm dw}-f_0$ and $T-T_{\rm MCT}$ with slope $\gamma(\rho)/\alpha$. As a consistency check we plot $f_{\rm dw}-f_0$ and $T-T_{\rm MCT}$ and find that, within the numerical error, our calculations support this expectation (Fig. 9).

At first sight, one might expect that if D is related to a property of the PES, then $D\sim(f_{\rm dw})^{\alpha}$, i.e., that $f_0\approx 0$. To explain why $f_0\neq 0$, we recall the discussion in Sec. II B, where we underline how a double-well mode may not contribute to diffusion.

To test whether the small fraction f_0 of double-well modes is indeed related to diffusivity, we have further scrutinized every double-well mode following the procedure suggested in Refs. [30,40]; for each double-well mode, we perform a potential energy minimization starting from the two apparent one-dimensional minima and locate the two associated local potential energy-minimum configurations (the inherent structures) [20]. The minimization is performed implementing a conjugate gradient algorithm with tolerance 10^{-15} kJ/mol [50]. The distance between the two quenched configurations is calculated as

$$d=\sqrt{\sum_{i=1}^{3N}(\mathbf{r}_i^1-\mathbf{r}_i^2)^2/(3N)}, \qquad (4)$$

where $\mathbf{r}_i^{\beta}$ is the ith atom position in the inherent structure β and N is the number of molecules. We have performed more than 50 000 minimizations.

Figure 10 shows a histogram of the distance d between the two inherent structure configurations obtained by conjugate gradient minimization. The histogram is characterized by a bimodal distribution, as previously found for Lennard-Jones liquids [27], with peaks separated by more than one order of magnitude. We associate the left peak, centered around $d=0.004$ nm, with nondiffusive directions. Indeed, the difference of the distance d between these two configurations $\beta=1$ and $\beta=2$ is so small that if they differed by the displacement of only one molecule, then the displacement of the center of mass of this one molecule would be ≈ 0.06 nm, i.e., about 1/5 of the nearest neighbor distance, which is about 0.28 nm.

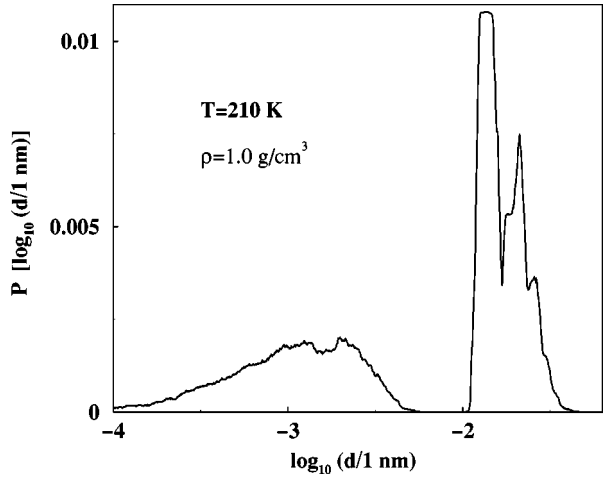

FIG. 10. Histogram of the distance d defined in Eq. (4) between the two inherent structure configurations associated with the two minima along one straight path eigendirection. Here d is measured in nm.

According to Refs. [30,40], we classify the modes contributing to this left peak as ''false'' (or nondiffusive) double-well modes, and focus only on the remaining directions in configuration space, which we call ''escape'' directions. In Fig. 11 we show a parametric plot of $D^{1/2}$ versus the fraction of escape directions $f_{\rm esc}$. The dependence of D on $f_{\rm esc}$ appears still to be well represented by the same power law of Eq. (3), where the fitting parameter f_0 is reduced by more

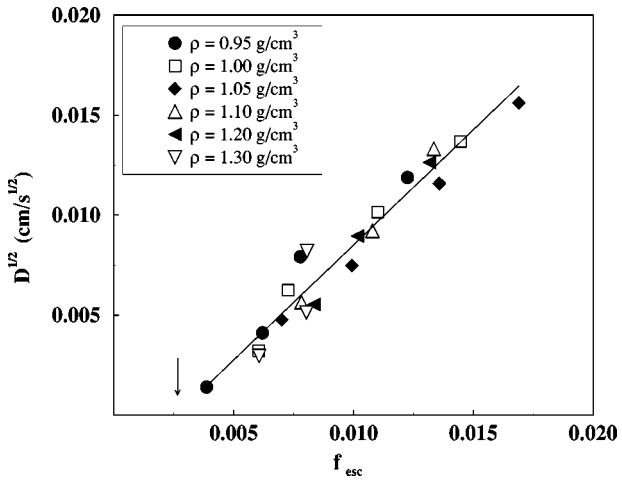

FIG. 11. Parametric plot of $D^{1/2}$ versus $f_{\rm esc}$, the fraction of the escape directions. The arrow denotes $f_0\approx 0.003$.

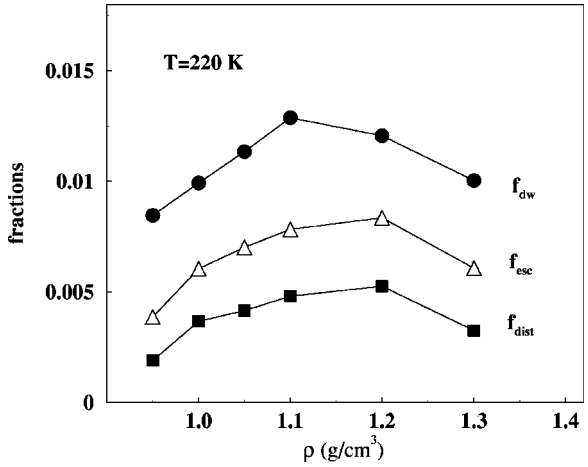

FIG. 12. Density dependence of f_{dw}, f_{dist}, and f_{esc} at one selected temperature $T=220$ K.

than a factor of 2, but still is not zero. The small number of escape directions results in poorer statistics than obtained for the double-well data (Fig. 8). Following Ref. [27], we also evaluate the total number of distinct basins which can be reached along every escape direction. The number of distinct basins—normalized by $6N-3$ to be consistent with the normalization of f_{dw} and f_{esc}—is called f_{dist}.

The density dependences of f_{dw}, f_{dist}, and f_{esc} at one selected T are shown and compared with f_{dw} in Fig. 12. Note that all three curves have similar behavior. The T dependence of f_{dw}, f_{esc}, and f_{dist} is shown in Fig. 13(a) for one density. We linearly extrapolate all the quantities to zero to calculate the locus where $f_{dw}=0$, the locus where $f_{esc}=0$, and the locus $f_{dist}=0$. The last two loci coincide within the errors. We note that for most densities and temperatures studied, $f_{dw}-f_{esc}=0.0045\pm0.0025$ [Fig. 13(b)], accounting within the numerical error for the nonzero value of f_0.

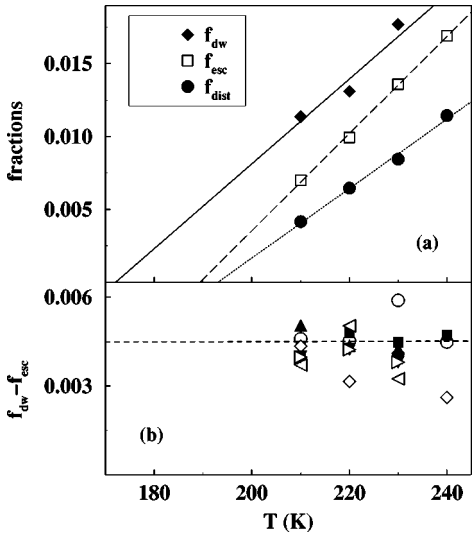

FIG. 13. (a) T dependence of the fraction of double-well, escape and distinct directions f_{dw}, f_{esc}, and f_{dist} density: $\rho=1.05$ g/cm^3. (b) $f_{dw}-f_{esc}$ for all densities as a function of T(○ $\rho=0.95$ g/cm^3; □ $\rho=1.0$ g/cm^3; ◇ $\rho=1.05$ g/cm^3; △ $\rho=1.1$ g/cm^3; ◁ $\rho=1.2$ g/cm^3; ∇ $\rho=1.3$ g/cm^3).

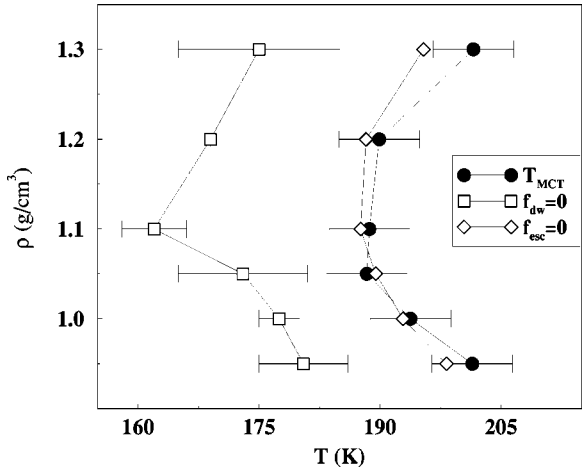

FIG. 14. Locus $f_{dw}=0$ and $f_{esc}=0$ in the T,ρ plane and the ρ dependence of the ideal MCT critical temperature, previously calculated for the same potential T_{MCT} [12].

We next compare in Fig. 14 the locus $f_{esc}=0$ in the (T,ρ) plane with the ρ dependence of T_{MCT} [12]. We also report the T at which the fraction f_{dw} of double-well modes vanishes. We find that the locus of $f_{esc}=0$ nearly coincides with the T_{MCT} line, while the $f_{dw}=0$ locus tracks the T_{MCT} line, but it is shifted to lower temperature.

The coincidence of $f_{esc}=0$ with T_{MCT} is particularly relevant. First of all, it confirms that the quantity f_{esc} is a good measure of the diffusive modes, supporting the validity of our mode classification. Second, and perhaps more important, this coincidence strengthens the hypothesis that the ideal MCT critical temperature is the temperature at which free exploration of configuration space is not possible any longer. This statement is consistent with the general consensus that the dynamical processes above and below T_{MCT} are different. The reduction of mobility on cooling appears to be related to the properties of the PES. The system mobility is reduced because the number of directions that connect different local minima and allow the system to *freely* explore the configuration space is decreasing [51]. Hence, the observed reduced mobility is ''entropic'' in origin. Since in the studied (ρ,T) range MCT provides a good description of the dynamics, this implies that MCT is able to describe the entropic slowing down of the dynamics associated with the vanishing of f_{esc}.

In a recent work [6], we investigated the relation between diffusion and configurational entropy. In the formalism introduced by Stillinger and Weber [20], the configurational entropy is a measure of the logarithm of the number of different basins $\Omega(T,\rho)$ in configuration space sampled by the system in equilibrium. We have found that the slowing down of the dynamics correlates with the decrease of configurational entropy.

The fact that both $\Omega(T,\rho)$ and the number of free directions are strongly tied to diffusion suggests the possibility of a direct relation between the two quantities. The simplest possibility is that each of the sampled basins is connected to all other $\Omega(T,\rho)$ basins, i.e., f_{esc} is proportional to Ω or $\log(f_{esc})\sim S_{conf}$. This possibility is consistent with our data

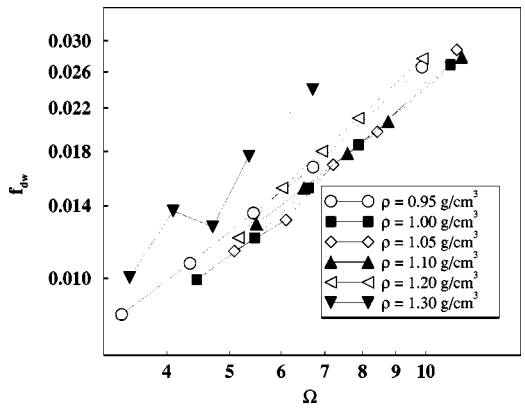

FIG. 15. Log-log plot of f_{dw} vs Ω for all studied densities [55].

(Fig. 15). Note that the same relation has been recently derived in the framework of a random energy model (REM) for supercooled liquids [52].

V. CONCLUSIONS

The calculations presented here provide evidence that two different dynamical mechanisms affect the slowing down of the dynamics in supercooled states.

(i) In the weakly supercooled region, the slowing down of the dynamics arises from the progressive reduction in the number of directions where free exploration of configuration space is possible. The system is always located close to a multidimensional ridge between different basins, and the time scale of the long-time dynamics is set by the time required to probe one of the free directions. In this range of T, the diffusion is not limited by the presence of energy barriers that must be overcome by thermally activated processes, but is controlled by the limited number of directions leading to different basins along almost constant potential energy paths [21]. As shown in Fig. 8, independent from the density, the number of free directions completely determines the value of D.

(ii) Close to the MCT critical temperature, the system starts to sample regions of configuration space that have no free directions. The change in the dynamics above and below T_{MCT} can be viewed as a change in the properties of the PES sampled in equilibrium, from configurations always close to a ridge of progressively lower dimension to configurations far from any ridge [29,21]. Below T_{MCT}, the system must go close to the ridge and then select the right direction. The search for the ridge below T_{MCT}, i.e., the search for a rare event, can be probably described as an activated process. More work is required in this direction [53]. Current computer facilities are beginning to explore the region below T_{MCT}, and detailed information on the dynamics, and on the properties of the PES sampled below T_{MCT} in simple models, will be hopefully available.

Finally, the relation between connectivity and number of local minima in the PES (Fig. 15)—which can be calculated in theoretical models as recently done for the random energy model (REM) [52]—may help build on the existing ideas bridging thermodynamics and dynamics [54]. It will be important to verify if the same relation holds also for different models of liquids and, in particular, to study the validity of this relation above and below T_{MCT}.

ACKNOWLEDGMENTS

We thank T. Keyes and G. Ruocco for helpful discussions, and NSF Grant No. CHE9728874 for support. F.S. acknowledges partial support from MURST (COFIN 2000) and INFM (PRA-HOP and Iniziativa Calcolo Parallelo).

[1] K. Binder *et al.*, in *Complex Behavior of Glassy Systems*, edited by M. Rubi and C. Perez-Vicente (Springer Berlin 1997); W. Kob, J. Phys.: Condens. Matter **11**, A1 (1999).
[2] A. Heuer, Phys. Rev. Lett. **78**, 4051 (1997).
[3] S. Sastry, P. G. Debenedetti, and F. H. Stillinger, Nature (London) **393**, 554 (1998).
[4] F. Sciortino, W. Kob, and P. Tartaglia, Phys. Rev. Lett. **83**, 3214 (1999).
[5] T. Schrøder, S. Sastry, J. Dyre, and S. C. Glotzer, J. Chem. Phys. **112**, 9834 (2000).
[6] A. Scala, F. W. Starr, E. La Nave, F. Sciortino, and H. E. Stanley, Nature (London) **406**, 166 (2000).
[7] S. Sastry, Nature (London) **409**, 164 (2001).
[8] L. J. Lewis and G. Wahnström, Phys. Rev. E **50**, 3865 (1994).
[9] W. Kob and H. C. Andersen, Phys. Rev. E **51**, 4626 (1995); **52**, 4134 (1995).
[10] F. Sciortino, L. Fabbian, S.-H. Chen, and P. Tartaglia, Phys. Rev. E **56**, 5397 (1997).
[11] M. C. Ribeiro and P. A. Madden, J. Chem. Phys. **108**, 3256 (1998), and references therein.
[12] F. W. Starr, S. Harrington, F. Sciortino, and H. E. Stanley, Phys. Rev. Lett. **82**, 3629 (1999); F. W. Starr, F. Sciortino, and H. E. Stanley, Phys. Rev. E **60**, 6757 (1999).
[13] M. Nauroth and W. Kob, Phys. Rev. E **55**, 657 (1997); T. Gleim, W. Kob, and K. Binder, Phys. Rev. Lett. **81**, 4404 (1998).
[14] L. Fabbian, R. Schilling, F. Sciortino, P. Tartaglia, and C. Theis, Phys. Rev. E **58**, 7272 (1998).
[15] W. Götze, J. Phys.: Condens. Matter **11**, A1 (1999); W. Götze, in *Liquids, Freezing and Glass Transition*, edited by J. P. Hansen, D. Levesque, and J. Zinn-Justin (North-Holland, Amsterdam, 1991).
[16] MCT calculations for SPC/E water are described in L. Fabbian, A. Latz, R. Schilling, F. Sciortino, P. Tartaglia, and C. Theis, Phys. Rev. E **60**, 5768 (1999); **62**, 2388 (2000); C. Theis, A. Latz, R. Schilling, F. Sciortino, and P. Tartaglia, *ibid.* **62**, 1856 (2000).
[17] MCT calculations for SiO_2 (BKS potential) are described in F. Sciortino and W. Kob, Phys. Rev. Lett. **86**, 648 (2001).
[18] J. Horbach and W. Kob, Phys. Rev. B **60**, 3169 (1999).
[19] H. Jonsson and H. C. Andersen, Phys. Rev. Lett. **60**, 2295 (1988).

[20] F. H. Stillinger and T. A. Weber, Science **225**, 983 (1984).
[21] L. Angelani, R. Di Leonardo, G. Ruocco, A. Scala, and F. Sciortino, Phys. Rev. Lett. **85**, 5356 (2000).
[22] E. La Nave, A. Scala, F. W. Starr, F. Sciortino, and H. E. Stanley, Phys. Rev. Lett. **84**, 4605 (2000).
[23] T. Keyes, J. Phys. Chem. A **101**, 2921 (1997).
[24] W. Li and T. Keyes, J. Chem. Phys. **111**, 5503 (1999).
[25] T. Keyes, J. Chem. Phys. **101**, 5081 (1994).
[26] M. Goldstein, J. Chem. Phys. **51**, 3728 (1969).
[27] C. Donati, F. Sciortino, and P. Tartaglia, Phys. Rev. Lett. **85**, 1464 (2000).
[28] S. Bembenek and B. Laird, Phys. Rev. Lett. **74**, 936 (1995).
[29] F. Sciortino and P. Tartaglia, Phys. Rev. Lett. **78**, 2385 (1997).
[30] J. D. Gezelter, E. Rabani, and B. J. Berne, J. Chem. Phys. **107**, 4618 (1997).
[31] K. Broderix, K. K. Bhattacharya, A. Cavagna, A. Zippelius, and I. Giardina, Phys. Rev. Lett. **85**, 5360 (2000).
[32] By definition, a saddle of order 0 is a minimum, while a saddle of order 1 is a normal saddle.
[33] H. J. C. Berendsen, J. R. Grigera, and T. P. Straatsma, J. Phys. Chem. **91**, 6269 (1987).
[34] F. Sciortino, Chem. Phys. **258**, 295 (2000).
[35] F. X. Prielmeier, E. W. Lang, R. J. Speedy, and H.-D. Ludemann, Phys. Rev. Lett. **59**, 1128 (1987).
[36] D. J. Wales, J. Chem. Phys. **113**, 3926 (2000).
[37] For a recent application of INM in the interpretation of the short time dynamics see, for example, A. Ma and R. M. Stratt, Phys. Rev. Lett. **85**, 1004 (2000), and references therein.
[38] W. Li, T. Keyes, and F. Sciortino, J. Chem. Phys. **108**, 252 (1998).
[39] M. Buchener and T. Dorfmüller, J. Mol. Liq. **65/66**, 157 (1995).
[40] S. D. Bembenek and B. B. Laird, J. Chem. Phys. **104**, 5199 (1996).
[41] The participation ratio p_α, is defined as $p_\alpha=[N\Sigma(e_j^\alpha \dot{e}_j^\alpha)]^{-1}$, where e_j^α is the normalized eigenvector, j runs over all the components of the system and α labels the modes. p_α gives a measure of the numbers of the molecules involved in the motion along the α eigenmode.
[42] R. L. Murry, J. T. Fourkas, W. X. Li, and T. Keyes, J. Chem. Phys. **110**, 10 410 (1999); **110**, 10 423 (1999).
[43] F. W. Starr, S. Sastry, E. La Nave, A. Scala, H. E. Stanley, and F. Sciortino, Phys. Rev. E **63**, 041201 (2001).
[44] LAPACK is a library of Fortran 77 subroutines for solving the most commonly occurring problems in numerical linear algebra. The name LAPACK is an acronym for linear algebra package. A list of LAPACK Frequently Asked Questions (FAQ) is maintained at URC http://www.netlib.org/lapack/.
[45] M. Cho, G. R. Fleming, S. Saito, and I. Omine, J. Chem. Phys. **100**, 6672 (1994).
[46] C. A. Angell, Science **267**, 1924 (1995).
[47] A. W. Kauzmann, Chem. Rev. **43**, 219 (1948).
[48] G. Seeley, T. Keyes, and B. Madan, J. Chem. Phys. **95**, 3847 (1991).
[49] P. Moore and T. Keyes, J. Chem. Phys. **100**, 6709 (1994).
[50] W. H. Press *et al.*, *Numerical Recipes in Fortran 77* (Cambridge University Press, Cambridge, 1992).
[51] R. Botet *et al.*, in *Universalities in Condensed Matter*, edited by R. Jullien, L. Peliti, R. Rammal, and N. Boccara (Springer Verlag, Berlin, 1987) p. 250.
[52] T. Keyes, Phys. Rev. E **62**, 7905 (2000).
[53] M. Sasai, Physica A **285**, 315 (2000).
[54] G. Adam and J. H. Gibbs, J. Chem. Phys. **43**, 139 (1965).
[55] Note that in Fig. 5 of Ref. [22] the value of the configurational entropy was underestimated by a constant value of 0.65. We have corrected this error in the present version of the figure.